Time-resolved high-temperature detection with single charge resolution of holes tunneling into many-particle quantum dot states

T. Nowozin,[1,*] A. Marent,[1] G. Hönig,[1] A. Schliwa,[1] D. Bimberg,[1] A. Beckel,[2] B. Marquardt,[2] A. Lorke,[2] and M. Geller[2]

[1]*Institut für Festkörperphysik, Technische Universität Berlin, Hardenbergstrasse 36, 10623 Berlin, Germany*

[2]*Laboratorium für Festkörperphysik and CeNIDE, Universität Duisburg-Essen, Lotharstrasse 1, 47048 Duisburg, Germany*

We demonstrate detection of many-particle hole states in InAs/GaAs quantum dots with single charge resolution up to a temperature of 75 K. Capacitance-voltage measurements as well as time-resolved current measurements in an adjacent two-dimensional hole gas are used to determine the emission and capture time constants from 4 K up to 130 K. A transition from pure tunneling to thermally assisted tunneling is observed with increasing temperature. An equivalent circuit model gives access to the energy level splittings of the many-particle hole states and explains the broadening of the peaks at higher temperatures.

I. INTRODUCTION

Due to their discrete density of states, self-organized quantum dots (QDs) exhibit electronic and optical properties which make them qualitatively distinct from higher dimensional semiconductor heterostructures.[1] Based on a decade of research of their fundamentals, many novel or improved devices were demonstrated, leading to their first application in systems. Among these devices are high-speed QD lasers[2,3] and amplifiers, single-photon emitters,[4] and QD-based Flash memories.[5–8] The superior functionality of these devices is predominantly based on the particular excitonic or electronic properties of QDs like tunable exchange interaction.[9] Remarkably, holes which are also strongly localized in QDs were studied in detail only recently using excitation spectroscopy,[10,11] although they are of great interest, for example, for quantum information processing[12] using single-hole spin states[13] at temperatures higher than 4 K or for novel memories.[14]

Capacitance-voltage (C-V) measurements have proven to be a valuable tool for determining the electronic structure of an ensemble of QDs like localization energies or the capture and emission dynamics for both electrons and holes.[14–20] For single QDs defined by electron beam lithography, single-electron spectroscopy was developed by using adjacent quantum point contacts (QPCs).[21–23] This method is presently used exclusively at low temperatures (typically in the 100-mK range) due to the weak spatial confinement and the resulting small level spacing (typically 1 meV) in lithographically defined QDs.

Recently, a different method has been proposed which enables charge detection in QDs at temperatures higher than a few millikelvins.[24–26] A two-dimensional system, either a 2DEG or a 2DHG, is placed in the vicinity of a layer of self-organized QDs. The charges confined inside the QDs deplete the number of free charge carriers and reduce the mobility in the 2D system and hence reduce the conductance, easily detected via a current measurement. The much higher localization energy of carriers in self-organized QDs compared to lithographically defined QDs provides a level splitting large enough to detect single-charge states at much higher temperatures than hitherto, possibly up to room temperature. Furthermore, conductance measurements in a 2D gas pave the

way to scaling the device size down to the nanometer range containing just a few or a single QD.

In this paper, we indeed present detection of a sequence of single- and many-particle hole states in self-organized QDs by an adjacent 2DHG at temperatures well above the helium temperature up to 75 K. The 2DHG is demonstrated to be an efficient and sensitive detector for study of both tunnel emission from QDs into the 2DHG and tunnel capture of holes into QDs from the 2DHG. The transients observed in time-resolved conductance measurements are monoexponential and time constants are easily derived. From an equivalent circuit model the energy level splittings of many-particle hole states are determined. In addition, the lever arm (ratio of gate voltage change to potential change at the position of the QDs, which is needed to derive the energies of the hole states) is calculated, taking into account the gate voltage and the number of holes confined inside the QDs.

II. SAMPLES

We study two types of structures grown by molecular beam epitaxy (MBE), which are almost identical except for a different tunnel barrier width. The schematics of the structures is shown in Fig. 1. One InAs/GaAs QD layer, with a nominal QD density of 3×10^{10} cm^{-2}, is embedded in a GaAs quantum well (QW) inside a nominally undoped Al$_{0.9}$Ga$_{0.1}$As matrix. Underneath the QD layer a 2DHG is formed in 8-nm GaAs, with holes provided by an adjacent 30 nm wide, 2×10^{18} cm^{-3}, p-doped layer. Structure A has a 5-nm-thick Al$_{0.9}$Ga$_{0.1}$As barrier between the QD layer and the 2DHG, while the barrier in structure B is 10 nm thick. The total tunneling length from the QD ground state amounts to 18 and 23 nm, respectively. Ohmic source and drain contacts were formed by thermal evaporation of a Ni/Zn/Au alloy and subsequent annealing to contact the 2DHG layer. The Schottky gate contact was made of a Ni/Au alloy after the annealing step. Samples were processed by chemical wet-etching into Hallbar mesa structures with an effective gate area of 740×310 μm^2.

Transfer length measurements (TLM) at room temperature yield a sheet resistance of 12 800 Ω and a specific contact resistance of 1.06×10^{-5} Ω m^2 for structure B. Hall measurements show a mobility for structure B of 191 cm^2/Vs and a
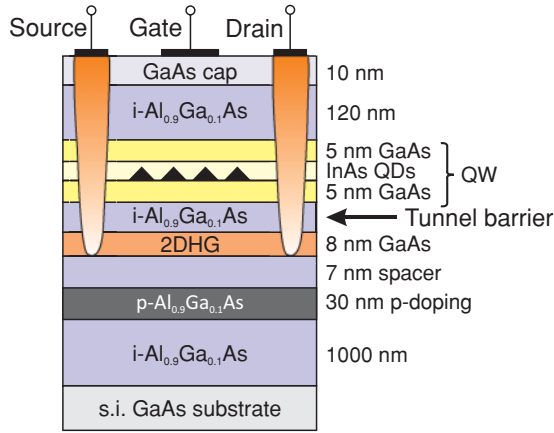
FIG. 1. (Color online) Schematics of the modulation-doped field effect transistor (MODFET) structure with an embedded layer of InAs QDs. The total width of the tunnel barrier is 18 nm (5 nm $Al_{0.9}Ga_{0.1}As$ and 13 nm GaAs) in structure A and 23 nm (10 nm $Al_{0.9}Ga_{0.1}As$ and 13 nm GaAs) in structure B.

sheet density of 2.26×10^{12} cm^{-2} at 300 K and 2010 cm^2/V s and a sheet density of 1.59×10^{12} cm^{-2} at 77 K, respectively.

The valence band structures calculated with a Poisson Solver[27] at a temperature of 25 K around the position of the QDs are depicted in Fig. 2 for a set of selected gate voltages. The total localization energy of the holes in the structure has been taken from deep-level transient spectroscopy (DLTS) measurements on similar QDs as 710 meV [210 meV for the QDs and about 500 meV for the band offset between GaAs and $Al_{0.9}Ga_{0.1}As$; see Fig. 2(a)].[14]

III. C-V MEASUREMENTS

A standard tool for study of the properties of electrons and holes in QDs is a C-V measurement.[28–31] The differential capacitance ($C = dQ/dV$) is equivalent to the amount of charge that is transferred by an ac voltage, which is superimposed to a constant gate dc bias. Here, the samples are designed in such a way that, by applying a gate bias, the energy levels of the QDs (i.e., the peaks in the QD density of states) can be energetically aligned with the Fermi level in the 2DHG (see calculated valence band structures in Fig. 2). This means that whenever a peak in the density of states of the QDs becomes aligned with the 2DHG quasi-Fermi level, C will increase due to the increased tunneling probability. The 2DHG itself is assumed to follow the applied gate bias instantaneously and thus is in thermal equilibrium at all times during the measurement.

Figure 3 depicts the gate-source capacitance measurements of structure A. The dc gate bias was swept between 2 and -0.5 V, subsequently filling up the QDs, whereas the ac amplitude was set to 5 mV. The measurements were performed at temperatures ranging from 4.2 to 100 K at a frequency of 1014 Hz.

In total, six peaks are clearly visible in Fig. 3 up to a temperature of 50 K. Even at a temperature of 100 K the two peaks at the largest gate bias (peaks 1 and 2) can be observed.

At 1.35 V (peak 1) the ground state of the QD ensemble is filled by one hole. The ground state is twofold degenerate. A second hole added to the ground state of a QD has to overcome
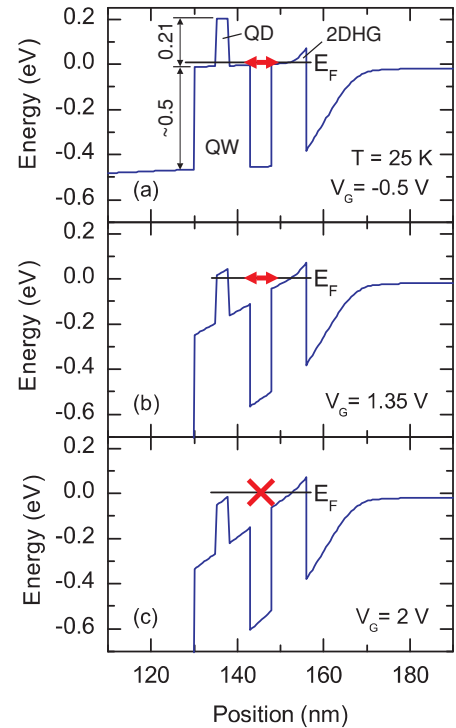

FIG. 2. (Color online) Calculated valence band structures around QDs for selected gate voltages V_G at 25 K for structure A. (a) The Fermi level E_F is above the energy levels of the QDs. (b) The Fermi level E_F is at the first energy level of the QDs, corresponding to peak 1 in Fig. 3. (c) The Fermi level E_F is below the energy levels of the QDs (no tunneling).

the Coulomb repulsion by the first hole, leading to a shift of the (unoccupied) energy level to higher energies. Hence, the second hole per QD will transfer to the QDs at a gate bias of 1.1 V (peak 2). Each additional hole adds to this Coulomb repulsion and shifts the energy levels to higher energies with respect to the unoccupied energy levels.[32] Further decreasing the gate bias leads to a filling of further higher energy levels in the QD ensemble (peak 3 to peak 6). Hence, the peaks belong to the many-particle hole states of QDs filled with one to six holes.
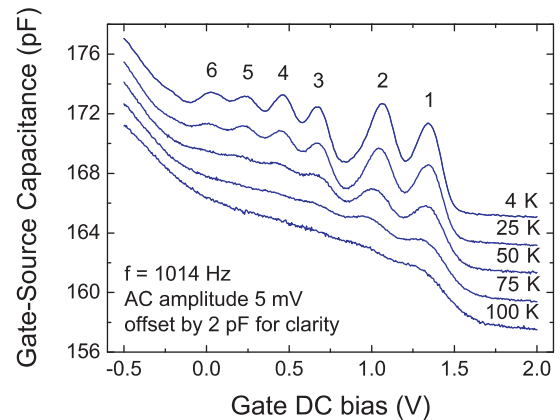

FIG. 3. (Color online) C-V measurements on structure A. Distinct peaks are visible up to a temperature of 100 K, corresponding to many-particle hole states in the QDs.

When the ac frequency is changed to values below 1014 Hz the amplitudes of the C-V curves saturate. In contrast, when the ac frequency is set to values higher than 1014 Hz the amplitudes of the C-V curves decrease and the peaks vanish at a frequency of about 15 kHz (not shown). The estimated cutoff frequency for the device RC low-pass is about 20 kHz and can be seen as a hint that the processes governing the time constants are not the tunneling emission and capture, but the parasitics of the device. The real cutoff frequency should be even lower than the estimate (less than half the value).

A Gaussian fit yields an area under the first peak of $\Delta C dU = 1.2 \times 10^{-12}$ CV. Multiplying it with an estimated geometric lever arm of $\lambda \approx 156$ nm/18 nm = 8.7 and dividing it by the elementary charge and the active gate area yields a hole density in the QD layer of 2.8×10^{10} cm^{-2}, which is in good agreement with the nominal QD density of the structures.

IV. 2DHG CURRENT MEASUREMENTS

C-V measurements give access to the static energy levels of many-particle hole states in QDs. Carrier dynamics can be investigated by time-resolved measurements of the 2DHG. The gate bias is swept in 10-mV steps, and at each step a pulse of 50 mV is applied to change the energetic position of the QDs relative to the 2DHG quasi-Fermi level. The holes that are transferred by the pulse from the 2DHG to the QDs reduce the conductance of the 2DHG and can thus be measured via changes of the current. A time-resolved source-drain current measurement for structure A with a source-drain voltage of 5 mV is shown in Fig. 4. The transients display the emission and capture processes related to peak 1 in Fig. 3. The emission of holes from the QDs to the 2DHG occurs when the energy level in the QD moves above the quasi-Fermi level of the 2DHG, leading to a rise in the current. Capture of holes by the QDs takes place when the quasi-Fermi level of the 2DHG is above the unoccupied levels of the QDs, leading to a reduction in the current.

The amplitude of the transients corresponds to the number of holes which are transferred during the pulse. Hence, as in the C-V measurements, by plotting the amplitude versus the gate
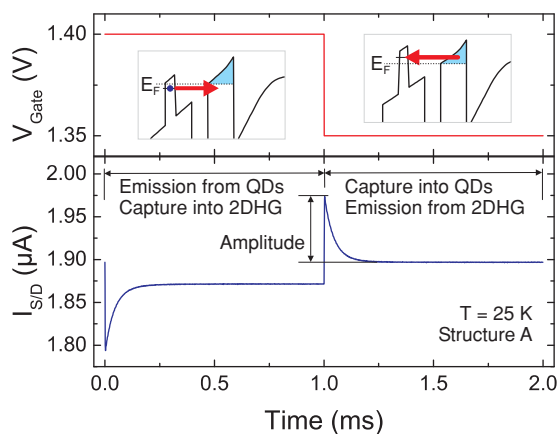

FIG. 4. (Color online) Structure A: Emission and capture transients in the source-drain current as a result of a gate pulse. The amplitude is a measure of the amount of charge which is transferred between QDs and 2DHG during the pulse.
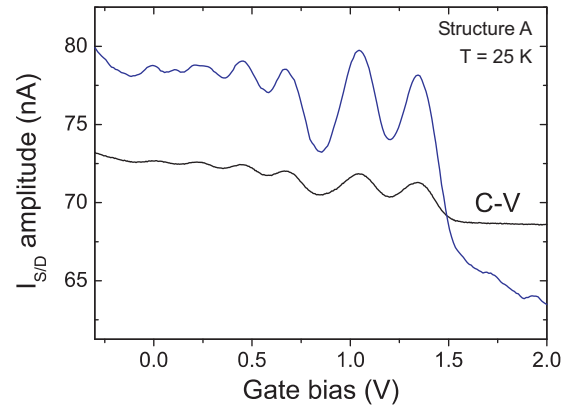

FIG. 5. (Color online) Emission source-drain current ($I_{S/D}$) transient amplitudes plotted versus the respective gate voltage for structure A. The curve is smoothed by a Savitzky-Golay algorithm with a fit window of 100 mV. The spectrum resembles the peak structure in the C-V curves [see lower (black) curve for comparison].

bias, distinct peaks appear at voltages where the energy levels of the QDs align with the quasi-Fermi level of the 2DHG. Figure 5 shows the amplitudes at the respective gate voltages, ranging from -0.25 to 2 V. Again, in total, six peaks can be observed and the C-V curve at 25 K in Fig. 3 is exactly reproduced [lower (black) curve in Fig. 5]. However, due to the already mentioned RC low-pass cutoff frequency of structure A, the time constants of the transients cannot be evaluated since they are controlled by the RC low-pass of the device.

The situation is completely different for structure B, where the tunnel barrier is thicker. As a consequence, structure A shows a stronger coupling between the QDs and the 2DHG (small tunneling time constants), while structure B shows a weaker coupling (larger tunneling time constants). Due to the larger tunneling time constant, in the range of several seconds, C-V measurements are no longer feasible. The tunneling time constant, however, is now not limited by the RC cutoff frequency, and hence it can be investigated by current measurements of the 2DHG.

Again, the pulse offset is swept in small steps (10 mV), while the pulse amplitude is now set to 20 mV. The source-drain voltage is set to 30 mV. The emission and capture transients for a gate bias of 0.88 V are shown in Fig. 6 for a temperature of 4.2 K. The time constants of both transients are in the range of several tens of seconds, well above the time constant of the RC low-pass. Hence, the transients are directly related to the emission and capture processes. In Fig. 7 the amplitudes of the capture transients (see Fig. 6) are plotted versus the corresponding offset gate bias. Distinct peaks of the hole states in the QDs similar to the ones in the C-V measurements of structure A in Fig. 3 can be seen. The range of the gate bias voltage at which the peaks occur is reduced compared to that of structure A due to the thicker tunnel barrier, which alters the lever arm (ratio of gate voltage change to potential change at the position of the QDs) of the device.

When the temperature is increased above 4.2 K the peaks become less distinct, and they vanish completely above 70 K. Nevertheless, capture and emission transients can still be seen in the time-resolved measurements, as tunneling still takes
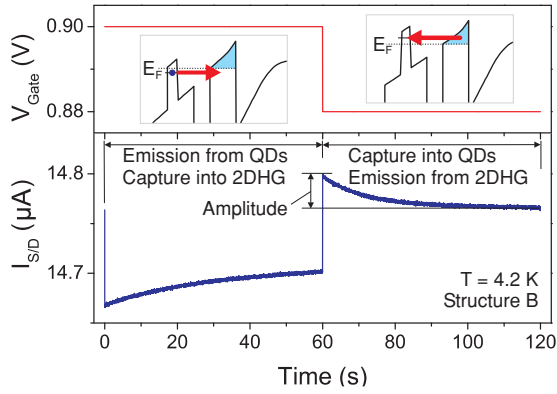
FIG. 6. (Color online) Structure B: source-drain current transients of emission of holes from the QDs into the 2DHG, and capture of holes from the 2DHG into the QDs. In this example the emission and capture are shown for gate voltages corresponding to peak 1 in the spectrum in Fig. 7, which corresponds to the ground state in the QD ensemble.

place between the QDs and the 2DHG. The drop in amplitude at the left in Fig. 7 for curves above 50 K comes from a drastic decrease in the capture time constants at these temperatures and gate biases. The capture processes in the upper levels become too fast for the measurement time window and the signal vanishes.

V. EMISSION AND CAPTURE TIME CONSTANTS

The emission and capture time constants for gate voltages corresponding to the peak positions in Fig. 7 are extracted from the transients by plotting them on a semilog scale and fitting the data as shown in Fig. 8 for the capture transient of peak 1 at 4.2 K. The emission and capture time constants for a set of different temperatures ranging from 4.2 to 130 K are shown in Fig. 9. From the temperature dependence of the time constants the dominant emission and capture processes can be identified.
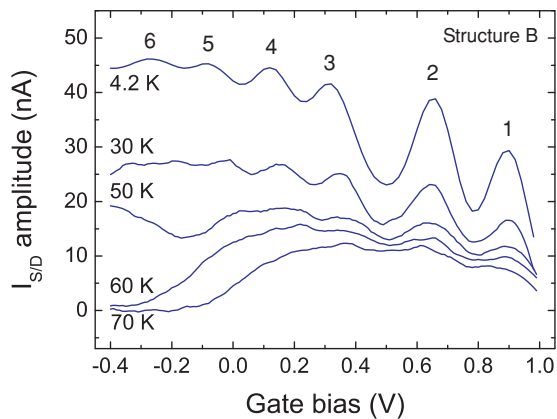

FIG. 7. (Color online) Structure B: Capture transient amplitudes plotted versus the gate bias at different temperatures. Curves have been smoothed with the Savitzky-Golay algorithm, with a fit window of 100 mV. As in Fig. 3 the QD features are still visible up to about 70 K.
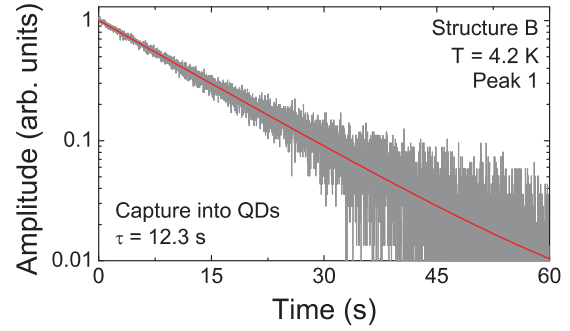

FIG. 8. (Color online) Structure B: Transient of hole capture into the QDs at the gate voltage corresponding to peak 1. The transients are monoexponential and allow an easy fit to extract the time constants.

At low temperatures, the time constants of all peaks are independent of the temperature but decrease for a lower gate bias, a clear sign of pure tunneling as the dominant emission and capture processes. When the temperature is increased the emission and capture time constants of the peaks at a low gate bias become smaller. Here, thermally assisted tunneling becomes the dominant emission and capture process.[33,34] The holes are thermally activated to a higher energy level and successively tunnel through the barrier. The emission and capture processes of the peaks at a higher gate bias (e.g., peak 1) are still governed by pure tunneling. For temperatures above 100 K the time constants also begin to drop for peak 1 and hence all emission and capture processes from the ground state to the higher states in the QDs are based on thermally assisted tunneling. Above temperatures of 130 K the emission
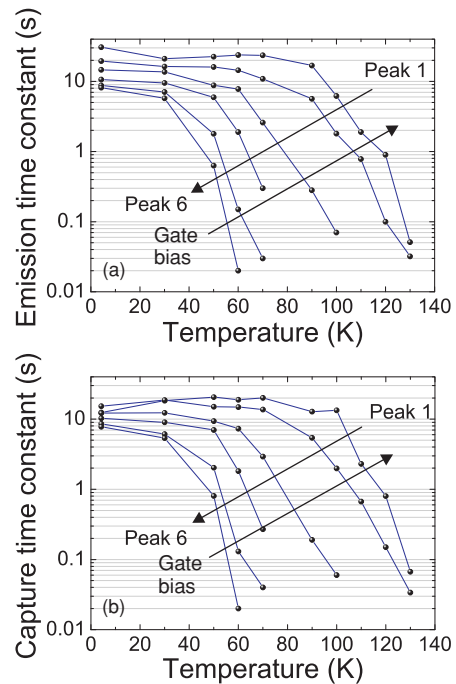

FIG. 9. (Color online) Structure B: (a) Emission and (b) capture time constants at the gate biases referring to the peak positions versus the temperature. The emission and capture processes become faster at higher temperatures due to enhanced thermally assisted tunneling.

and capture processes become too fast for the time scales used in our measurements.

The reason for the constant time constants of the emission and capture processes from/into the ground state (peak 1) up to a temperature of about 90 K is that temperature effects become less important for larger tunnel barriers. In contrast, higher states (peaks 3 to 6) have a smaller tunneling barrier and hence thermally assisted tunneling becomes more important for the emission process. Thus the time constants begin to decrease already at lower temperatures.[34] This temperature effect can also be seen in Fig. 7, where the peaks shift to higher gate voltages for increasing temperature, that is, the thermally assisted tunneling shifts the tunneling path slightly to higher energies and the same density of states is already measured for a higher gate bias.

VI. LEVEL SPLITTINGS OF MANY-PARTICLE STATES

The energy level splittings of the many-particle hole states in QDs can be obtained by using an equivalent circuit model for the device [see inset in Fig. 10(b)]. The device model is separated in constant geometric capacitances accounting for the MODFET structure and a potential-dependent quantum capacitance accounting for the density of states in the QD ensemble and the GaAs QW, in which the QD layer is embedded. The geometric capacitance is $C_{1,2} = \epsilon_r \epsilon_0 A / d_{1,2}$, with the relative dielectric constant ϵ_r, the vacuum electric constant ϵ_0, the active gate area A, and the distance d between the plates. $C_{1,2}$ is the geometric capacitance between the gate and the QD layer and between the QD layer and the 2DHG, respectively. The quantum capacitance is $C_q(E) = C_{QD} + C_{QW} = e^2[D_{QD}(E) + D_{QW}(E)]/A$, where e is the elementary charge, $D_{QD}(E)$ the density of states in the QD ensemble, $D_{QW}(E)$ the density of states in the QW, and A the active

gate area. The total capacitance of the device dependent on the potential energy E in the quantum region is then[35]

$$C_{tot}(E) = \cfrac{1}{\cfrac{1}{C_1} + \cfrac{1}{C_2 + C_q(E)}}. \tag{1}$$

The density of states in the QD ensemble is assumed to consist of six Gaussians accounting for the many-particle hole states. The increase in the capacitance at gate voltages below -0.2 V is well described by the slope of a Gaussian, which accounts for the density of states of the GaAs QW.

Equation (1) cannot be solved analytically without knowing the lever arm λ, which again depends on the total capacitance C_{tot}. The total capacitance can be expressed in terms of the lever arm λ, the charge Q, and the applied voltage U from Eq. (1) as

$$C_{tot}(E) = \frac{dQ}{dU} = \cfrac{1}{\cfrac{dU}{dQ_1} + \cfrac{1}{\cfrac{dQ_2}{dU} + \frac{e^2}{\lambda}(D_{QD} + D_{QW})}}, \tag{2}$$

with the lever arm $\lambda = \frac{e}{dE/dU} = \frac{1/C_{tot}}{1/(C_2 + C_q)}$. C_{tot} can now be obtained numerically by starting with a lever arm λ for empty QDs ($C_q = 0$). The bias voltage U will be stepwise increased by ΔU and the Fermi level will be calculated for $U + \Delta U$ using the value of the last-known lever arm. The new Fermi level will be used to obtain the density of states $D_{QD} + D_{QW}$ at E_F. The values obtained will be used to calculate the next total capacitance and lever arm, respectively. The peak positions in the QD density of states are then adjusted manually to fit the capacitance curve shown in Fig. 3. The full width at half maximum of the hole density of states is set manually to 9.2 meV, which is caused by the inhomogeneous broadening of the QD ensemble due to different values in size, composition, and shape of the QDs.

The density of states in the quantum region (QD ensemble and QW) per area $D_q(E)/A$ thus derived is shown in Fig. 10(a). The measured and calculated C-V curves are shown in Fig. 10(c), and the resulting lever arm in Fig. 10(b). The lever arm changes its value due to the charges which are added in the QDs when changing the gate bias. Before the 2DHG Fermi level passes the first state in the QDs, the lever arm is about 11, while after the last peak has passed, the lever arm has increased to a value of about 16. From Fig. 10(a) the energy level splittings of the many-particle hole states have been derived and are listed in Table I for structure A as well as for structure B. The main uncertainty of the values comes from the density of states assumed for the GaAs QW, in which the QD layer is embedded. As the effect of D_{QW} is stronger on the higher peaks (especially peaks 5 and 6), the uncertainty increases for the higher peaks. Calculations of the many-particle hole state energies in an InAs/GaAs QD model structure, using the Hartree-Fock approximation on top of the 8-band $\mathbf{k} \cdot \mathbf{p}$ theory,[36,37] reveal an excellent agreement of the many-particle level splittings with the experimental data (see Table I). The QD model structure used is a truncated pyramid of 20-nm base length and 3-nm height, with an average In composition of 90%.

At a temperature of 4.2 K, the temperature effect due to Maxwell-Boltzmann broadening of the Fermi function can be neglected. When increasing the temperature the broadening
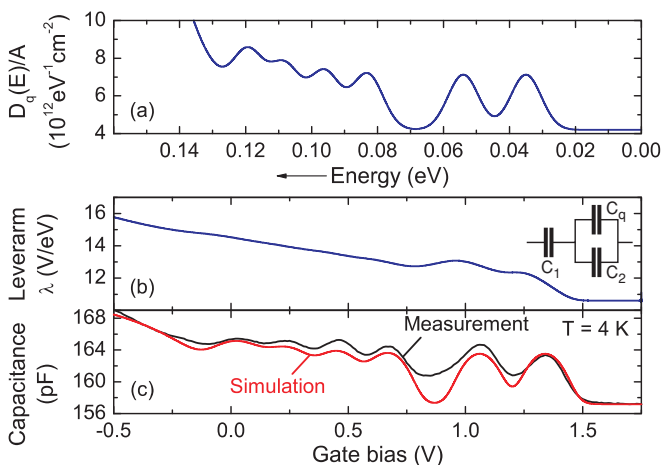

FIG. 10. (Color online) Structure A: (a) Density of states of the quantum region (QD ensemble and QW) per area $D_q(E)/A$ used in the simulation. (b) Occupation-dependent lever arm λ; the inset shows the equivalent circuit model. (c) Measured (black curve) and simulated (red curve) capacitance. Peak positions were manually adapted to fit the measured curve.

TABLE I. Energy level splittings of the many-particle hole states of structure A and structure B obtained using the equivalent circuit model with a quantum capacitance for the quantum region (QD ensemble and GaAs QW) at 4.2 K and values from the 8-band $\mathbf{k} \cdot \mathbf{p}$ theory.

Holes (peak no.)	Level splitting (meV)		
	Structure A	Structure B	8-band $\mathbf{k} \cdot \mathbf{p}$ theory
1–2	19 (1)	21 (1)	20.6
2–3	29 (1)	31 (1)	29.8
3–4	13 (1)	14 (1)	15.2
4–5	12 (2)	13 (2)	15.3
5–6	11 (2)	12 (2)	17.7

has to be included in the calculations. Assuming just one single sub-band in the 2DHG, the density of states is constant. We account for the broadening of the Fermi function by multiplying the density of states of the quantum region (QD ensemble and QW) $D_q(E)$ by the Fermi function $f(E, E_F, T)$ at the respective temperature T and gate voltage (which gives us E_F), then integrating the result from energies below the first QD level up to where the Fermi function has decayed sufficiently (i.e., from 0 to ∞), which gives us the total number of holes p_{tot} that can participate in the tunneling processes:

$$p_{\text{tot}}(E_F, T) = \int_0^\infty f(E, E_F, T) D_q(E) \, dE. \quad (3)$$

Next we take the derivative of p_{tot} for each energy to obtain a thermally broadened density of states in the quantum region:

$$D_{q, T > 4K}(E, T) = \left. \frac{d p_{\text{tot}}(E_F, T)}{d E_F} \right|_{E_F = E}. \quad (4)$$

With this thermally broadened density of states, the quantum capacitance and the total capacitance of the device are calculated as done before using Eqs. (1) and (2). The results are depicted in Fig. 11. Smearing-out of the individual peaks
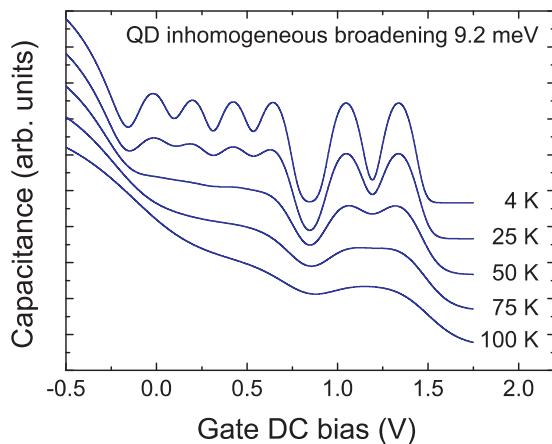

FIG. 11. (Color online) Influence of thermal broadening of the Fermi function at the position of the 2DHG on the simulated C-V curves of structure A. The smearing-out of the peaks compares qualitatively well with the measured curves (see Fig. 3).

can be seen. Similar to the measurements, the peak structure has vanished almost completely at a temperature of 100 K.

VII. DISCUSSION

C-V measurements and 2DHG current measurements have shown that a 2DHG is an excellent detector for many-particle hole states in QDs. The emission and capture processes for each individual hole state can be studied with single charge resolution. Furthermore, we are able to detect and discriminate the first two states in the QDs up to nitrogen temperature. Above that temperature no more peaks are resolved. The Fermi function is broadened at higher temperatures, leading to an energetic broadening of the 2DHG back contact as higher states show a higher occupation probability, thus distributing the fixed charge in the 2DHG across a wider span of energy levels, decreasing the energetic resolution.

Inhomogeneous broadening for a hole level due to fluctuations in the QD ensemble regarding size, shape, and composition could be determined, in the C-V simulation, to be as small as 9.2 meV.

When analyzing the potential of a 2DHG as a detector, we have to distinguish between two possibilities. First, the presence of holes in the QDs is detected. The spatial confinement of the holes within the GaAs QW (2DHG) in the vicinity of the QD layer improves the sensitivity, in contrast to an ordinary three-dimensional back contact, where the position of the contact varies with the applied gate voltage due to a change in the width of the depletion region. Second, different hole states in the QDs can be distinguished. This is enabled by the confinement of the holes and the resulting constant density of states in the 2DHG and the sharp Fermi level. While charge detection is still possible at room temperature (i.e., in ordinary Flash memories), the capability to discriminate the states is vanishing due to the broadening of the Fermi function.

VIII. CONCLUSION

We have demonstrated detection of many-particle hole states in InAs QDs with single charge resolution at temperatures up to 75 K. Distinct peaks in the C-V curves have been confirmed by time-resolved current measurements of an adjacent 2DHG. The peak structure vanishes above a temperature of 75 K, since the Maxwell-Boltzmann tail of the Fermi function in the 2DHG leads to an increased population of higher energy states. In 2DHG current measurements the time constants for the emission and capture processes could be extracted from the transients (ranging from about 10 s at 4 K to below 0.1 s above 100 K) and show the transition from pure tunnel emission/capture to phonon-assisted tunneling. An equivalent circuit model gave access to the energy level splittings of the many-particle hole states. The extracted values are in excellent agreement with 8-band $\mathbf{k} \cdot \mathbf{p}$ simulations.

ACKNOWLEDGMENTS

*Corresponding author: nowozin@sol.physik.tu-berlin.de

[1] D. Bimberg, ed., *Semiconductor Nanostructures* (Springer, Berlin, 2008).

[2] D. Bimberg, J. Phys. D **38**, 2055 (2005).

[3] C. Ribbat, R. L. Sellin, I. Kaiander, F. Hopfer, N. N. Ledentsov, D. Bimberg, A. R. Kovsh, V. M. Ustinov, A. E. Zhukov, and M. V. Maximov, Appl. Phys. Lett. **82**, 952 (2003).

[4] E. Stock, T. Warming, I. Ostapenko, S. Rodt, A. Schliwa, J. A. Töfflinger, A. Lochmann, A. I. Toropov, S. A. Moshchenko, D. V. Dmitriev, V. A. Haisler, and D. Bimberg, Appl. Phys. Lett. **96**, 093112 (2010).

[5] D. Nataraj, N. Ooike, J. Motohisa, and T. Fukui, Appl. Phys. Lett. **87**, 193103 (2005).

[6] C. R. Müller, L. Worschech, J. Heinrich, S. Höfling, and A. Forchel, Appl. Phys. Lett. **93**, 063502 (2008).

[7] A. Marent, T. Nowozin, J. Gelze, F. Luckert, and D. Bimberg, Appl. Phys. Lett. **95**, 242114 (2009).

[8] E. S. Kannan, G.-H. Kim, and D. A. Ritchie, Appl. Phys. Lett. **95**, 143506 (2009).

[9] R. Seguin, S. Rodt, A. Schliwa, K. Pötschke, U. W. Pohl, and D. Bimberg, Phys. Status Solidi B **243**, 3937 (2006).

[10] E. Siebert, T. Warming, A. Schliwa, E. Stock, M. Winkelnkemper, S. Rodt, and D. Bimberg, Phys. Rev. B **79**, 205321 (2009).

[11] T. Warming, E. Siebert, A. Schliwa, E. Stock, R. Zimmermann, and D. Bimberg, Phys. Rev. B **79**, 125316 (2009).

[12] T. D. Ladd, F. Jelezko, R. Laflamme, Y. Nakamura, C. Monroe, and J. L. OBrien, Nature **464**, 45 (2010).

[13] D. Heiss, S. Schaeck, H. Huebl, M. Bichler, G. Abstreiter, J. J. Finley, D. V. Bulaev, and D. Loss, Phys. Rev. B **76**, 241306(R) (2007).

[14] A. Marent, M. Geller, A. Schliwa, D. Feise, K. Pötschke, D. Bimberg, N. Akçay, and N. Öncan, Appl. Phys. Lett. **91**, 242109 (2007).

[15] B. T. Miller, W. Hansen, S. Manus, R. J. Luyken, A. Lorke, J. P. Kotthaus, S. Huant, G. Medeiros-Ribeiro, and P. M. Petroff, Phys. Rev. B **56**, 6764 (1997).

[16] C. M. A. Kapteyn, M. Lion, R. Heitz, D. Bimberg, P. N. Brunkov, B. V. Volovik, S. G. Konnikov, A. R. Kovsh, and V. M. Ustinov, Appl. Phys. Lett. **76**, 1573 (2000).

[17] D. Reuter, P. Kailuweit, A. D. Wieck, U. Zeitler, O. Wibbelhoff, C. Meier, A. Lorke, and J. C. Maan, Phys. Rev. Lett. **94**, 026808 (2005).

[18] A. Schramm, S. Schulz, J. Schaefer, T. Zander, C. Heyn, and W. Hansen, Appl. Phys. Lett. **88**, 213107 (2006).

[19] S. Schulz, A. Schramm, C. Heyn, and W. Hansen, Phys. Rev. B **74**, 033311 (2006).

[20] M. Geller, A. Marent, T. Nowozin, D. Bimberg, N. Akçay, and N. Öncan, Appl. Phys. Lett. **92**, 092108 (2008).

[21] L. M. K. Vandersypen, J. M. Elzerman, R. N. Schouten, L. H. W. v. Beveren, R. Hanson, and L. P. Kouwenhoven, Appl. Phys. Lett. **85**, 4394 (2004).

[22] S. Gustavsson, R. Leturcq, B. Simovi, R. Schleser, T. Ihn, P. Studerus, and K. Ensslin, Phys. Rev. Lett. **96**, 076605 (2006).

[23] S. Gustavsson, R. Leturcq, M. Studer, I. Shorubalko, T. Ihn, K. Ensslin, D. C. Driscoll, and A. C. Gossard, Surf. Sci. Rep. **64**, 191 (2009).

[24] B. Marquardt, M. Geller, A. Lorke, D. Reuter, and A. D. Wieck, Appl. Phys. Lett. **95**, 022113 (2009).

[25] M. Geller, B. Marquardt, A. Lorke, D. Reuter, and A. D. Wieck, Nanoscale Res. Lett. **5**, 829 (2010).

[26] B. Marquardt, M. Geller, B. Baxevanis, D. Pfannkuche, A. D. Wieck, D. Reuter, and A. Lorke, Nature Commun. **2**, 209 (2011).

[27] Nextnano [http://www.nextnano.de/nextnano3/]. Only the device was calculated, the quantum dots were added manually to the band structure afterward.

[28] P. Blood and J. W. Orton, *The Electrical Characterization of Semiconductors: Majority Carriers and Electron States* (Academic Press, London, 1992).

[29] P. N. Brounkov, A. Polimeni, S. T. Stoddart, M. Henini, L. Eaves, P. C. Main, A. R. Kovsh, Y. G. Musikhin, and S. G. Konnikov, Appl. Phys. Lett. **73**, 1092 (1998).

[30] C. M. A. Kapteyn, F. Heinrichsdorff, O. Stier, R. Heitz, M. Grundmann, N. D. Zakharov, D. Bimberg, and P. Werner, Phys. Rev. B **60**, 14265 (1999).

[31] R. Wetzler, A. Wacker, E. Schöll, C. M. A. Kapteyn, R. Heitz, and D. Bimberg, Appl. Phys. Lett. **77**, 1671 (2000).

[32] R. J. Warburton, B. T. Miller, C. S. Dürr, C. Bödefeld, K. Karrai, J. P. Kotthaus, G. Medeiros-Ribeiro, P. M. Petroff, and S. Huant, Phys. Rev. B **58**, 16221 (1998).

[33] G. Vincent, A. Chantre, and D. Bois, J. Appl. Phys. **50**, 5484 (1979).

[34] T. Nowozin, A. Marent, M. Geller, D. Bimberg, N. Akçay, and N. Öncan, Appl. Phys. Lett. **94**, 042108 (2009).

[35] M. Russ, C. Meier, A. Lorke, D. Reuter, and A. D. Wieck, Phys. Rev. B **73**, 115334 (2006).

[36] A. Schliwa, M. Winkelnkemper, and D. Bimberg, Phys. Rev. B **76**, 205324 (2007).

[37] C. Kindel, S. Kako, T. Kawano, H. Oishi, Y. Arakawa, G. Hönig, M. Winkelnkemper, A. Schliwa, A. Hoffmann, and D. Bimberg, Phys. Rev. B **81**, 241309(R) (2010).